Nanotechnology **21** (2010) 274008 (11pp) doi:10.1088/0957-4484/21/27/274008

Nanophotonics for quantum optics using nitrogen-vacancy centers in diamond

C Santori[1], P E Barclay[1], K-M C Fu[1], R G Beausoleil[1], S Spillane[2] and M Fisch[3]

[1] Information and Quantum Systems, HP Laboratories, 1501 Page Mill Road, Palo Alto, CA 94304–1123, USA
[2] Carnegie Mellon Silicon Valley, NASA Research Park, Building 23, Moffett Field, CA 94035-1000, USA
[3] College of Technology, Kent State University, Kent, OH 44242, USA

Received 1 December 2009, in final form 10 February 2010
Published 22 June 2010
Online at stacks.iop.org/Nano/21/274008

Abstract
Optical microcavities and waveguides coupled to diamond are needed to enable efficient communication between quantum systems such as nitrogen-vacancy centers which are known already to have long electron spin coherence lifetimes. This paper describes recent progress in realizing microcavities with low loss and small mode volume in two hybrid systems: silica microdisks coupled to diamond nanoparticles, and gallium phosphide microdisks coupled to single-crystal diamond. A theoretical proposal for a gallium phosphide nanowire photonic crystal cavity coupled to diamond is also discussed. Comparing the two material systems, silica microdisks are easier to fabricate and test. However, at low temperature, nitrogen-vacancy centers in bulk diamond are spectrally more stable, and we expect that in the long term the bulk diamond approach will be better suited for on-chip integration of a photonic network.

(Some figures in this article are in colour only in the electronic version)

1. Introduction

Diamond is an attractive material for some electronic and photonic applications because of its high thermal conductivity, excellent chemical stability and high carrier mobility [1]. Diamond appears to be an excellent material for quantum information and magnetic sensing applications as well, with hundreds of known optically active centers [2], many of which are paramagnetic. Few of these impurities have been studied in detail, but at least one of them, the nitrogen-vacancy (NV) center, is optically addressable and can exhibit electron spin coherence lifetimes exceeding 1 ms at room temperature [3]. This long-lived coherence is usually attributed to the nuclear spin-zero environment of the diamond lattice (^{12}C has 98.9% natural abundance) which can be further improved with isotopic purification. These capabilities have recently allowed for some remarkable demonstrations in this system such as controlled coupling between single electronic and nuclear spins [4, 5].

For quantum information applications, a logical next step would be to connect multiple diamond impurities such as NV centers together optically, to enable long-distance quantum communication through repeaters [6], or to test one-way quantum computation approaches [7]. However, currently it is rather difficult to fabricate structures such as waveguides and cavities in diamond. One of the chief difficulties at present is that one cannot commercially obtain a wafer containing a thin layer of high-quality single-crystal diamond on top of a lower-index insulator, analogous to silicon-on-insulator wafers. One can make similar structures by growing polycrystalline diamond on other materials, and optical structures have been made in this way [8], but these polycrystalline films have high scattering loss, and so far there are no reports of these films containing optically active impurities with good spin coherence properties. Nevertheless, there have been several recent efforts to surmount these problems using other approaches [9–14], and here we shall describe two such approaches attempted in our own laboratory, one based on coupling diamond nanoparticles to silica microdisk structures [15, 16], and the other based on higher-index gallium phosphide structures attached to bulk single-crystal diamond [17–19]. In both cases, coupling between NV centers and whispering-gallery-type cavity modes has been demonstrated. The most serious remaining technical challenges involve the properties of the NV centers in these structures.

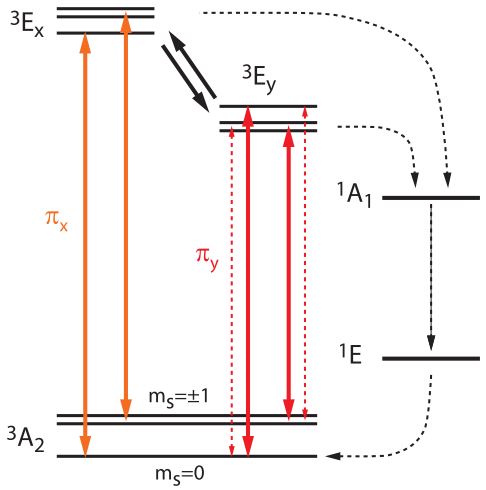

Figure 1. Schematic diagram showing the energy levels and optical transitions for a negatively-charged nitrogen-vacancy center in diamond, with a strain splitting between the E_x and E_y excited orbital states.

In this paper we begin by summarizing the relevant properties of the NV optical transitions. We also briefly discuss some theoretical issues related to spontaneous emission enhancement in hybrid cavity geometries. We then describe the fabrication and low temperature characterization of silica microdisk cavities coupled to diamond nanoparticles. Finally, we present theoretical and experimental studies of gallium phosphide structures coupled to NV centers in bulk diamond.

2. Optical transitions of NV$^-$

A schematic energy-level diagram for the electronic structure of the negatively-charged nitrogen-vacancy center (NV$^-$), as it is currently understood [20–22], is shown in figure 1. The NV center has trigonal symmetry (point group C_{3V}). The ground states, denoted as $^3A_2$, have an orbital singlet, spin triplet structure with a 2.87 GHz splitting between the $m_s = 0$ and ± 1 spin sublevels. These states are connected by optical transitions to a set of six excited states with an orbital doublet, spin triplet structure. Due to random strain fields present in the crystal, the orbital states denoted as E_x and E_y are typically nondegenerate. Here, x and y refer to principal axes in a plane perpendicular to the NV center, with an angle determined by the strain tensor. The magnitude of this splitting depends on the crystal quality, but in high-purity CVD-grown diamond it may be on the order of 10 GHz. The optical transitions involving the E_x and E_y orbital states follow linear polarization selection rules (π_x, π_y) as indicated. At low temperature, the E_x and E_y transitions can sometimes be spectrally resolved within the zero-phonon line. For the higher-energy orbital branch the $m_s = 0$ transition is primarily spin-conserving, useful as a cycling transition for spin readout. In the lower-energy orbital branch, non-spin-conserving transitions can be obtained [23, 24], useful for optical spin manipulation or for schemes based on Raman scattering.

Figure 2(a) shows a photoluminescence (PL) spectrum obtained from a dense ensemble of NV centers at liquid helium

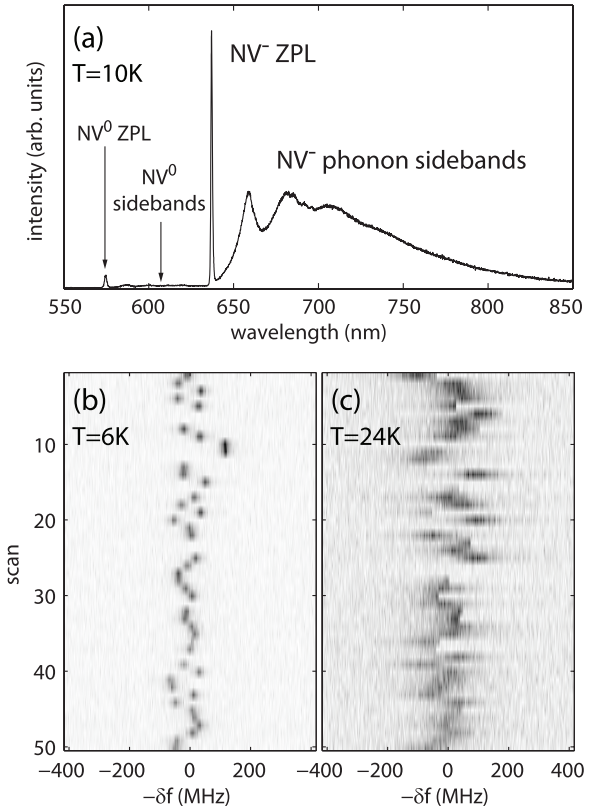

Figure 2. (a) Photoluminescence (PL) spectrum of a dense ensemble of NV centers under 532 nm excitation. (b) and (c) Photoluminescence excitation (PLE) measurements performed on a single NV center in high-purity CVD diamond, excited at a zero-phonon transition near 637 nm. The images represent total photoluminescence intensity collected from the longer wavelength phonon sidebands versus excitation frequency (x-axis), and repeated over many scans (y-axis), with dark colors indicating higher intensity. Short repump pulses (532 nm) were applied in between scans. The measurements were performed at (b) 6 K and at (c) 24 K.

temperature (10 K) under nonresonant excitation (532 nm) through the high-energy phonon sidebands. The main features are the zero-phonon lines of NV^0 and NV$^-$ at 575 nm and 637 nm, respectively, and the broad phonon sideband emission at longer wavelengths. It is clear in these spectra that the area contained within the sharp zero-phonon lines represents only a small fraction of the total emission (for NV$^-$ it is $\approx 3\%$). This small Debye–Waller factor is important to consider in quantum optics or cavity-QED applications. At room temperature, the main change that occurs in the PL spectrum is a broadening of the zero-phonon line to a width of several nanometers. The phonon sidebands show some subtle changes but appear qualitatively similar to those in figure 2(a).

In high-quality CVD-grown diamond, the inhomogeneous width of the zero-phonon line for an ensemble of NV centers can be as narrow as 10 GHz, but this is still a factor of 1000 larger than the natural linewidth of 13 MHz which has in fact been measured in single NV centers [25]. The linewidth of a single NV center can be measured by photoluminescence excitation (PLE) spectroscopy using a confocal microscopy setup. In this measurement, an external-cavity diode laser is scanned in frequency across one of the zero-phonon transitions

at ∼637 nm, while the resulting photoluminescence intensity into the phonon sidebands is measured with a photon counter. In between scans, a nonresonant excitation pulse at 532 nm is applied to reverse photoionization. Figure 2(b) shows PLE data obtained from a single NV center in an 'electronic-grade' CVD diamond sample, obtained commercially from Element 6, at a temperature of 6 K. As can be seen, the linewidth in each individual scan is below 20 MHz, but the center position of the resonance jumps randomly in each scan over a width of ∼100 MHz due to the effects of the repump laser. This amount of spectral diffusion, while still problematic for quantum applications, is better than what is seen in most types of natural or synthetic diamond. When the temperature is increased, the line broadens in each individual scan, as shown in figure 2(c). This broadening follows approximately a T^5 dependence up to 100 K [26]. Further experiments indicate that this broadening is caused by population transfer between the E_x and E_y orbital states through phonon scattering, and thus does not represent a pure dephasing process. At room temperature, this transfer between E_x and E_y is so rapid that only an effective, 'averaged' excited-state spin structure can be observed [27–29].

An important feature of NV^- at room temperature that has been critical in most experiments is that nonresonant excitation polarizes the spins into the $m_s = 0$ state, and furthermore the photoluminescence intensity depends on the degree of spin polarization obtained. The mechanism responsible for these effects is thought to be preferential relaxation of the $m_s = \pm 1$ excited states through spin singlet levels (^{1}E and ^{1}A$_1$ in figure 1), where population is trapped for some time before decaying preferentially to $m_s = 0$ [20]. The proper ordering of the spin singlet levels has been the subject of recent debate. The ordering shown in figure 1 follows [30].

From these properties we can see that there are two possible approaches for using a microcavity to enhance the optical transitions of the NV center. The first approach is to use a cavity with a low quality factor to enhance both the zero-phonon line and the phonon sidebands. Plasmonic cavities, waveguides or antennae, which have extremely small mode volumes, can indeed provide enhancement over the required >100 nm bandwidth. Promising results have already been achieved using gold nanoparticles to enhance the emission from NV centers in diamond nanoparticles [13]. This approach appears promising for nonresonant spin-state detection or for magnetometry, where the goal is simply to collect as much photoluminescence signal as possible. However, for schemes that create entanglement through single-photon generation and erasure of 'which-path' information [31], it is essential that the emitted photons be quantum mechanically indistinguishable, with a spectral bandwidth close to the lifetime limit. This means it is most likely that the device must be operated at low temperature (below 10 K), and even then only the 3% of emission that occurs into the zero-phonon line is useful. Thus, for entanglement generation schemes the goal should be to enhance only the zero-phonon line using a narrow linewidth (high quality factor) cavity. Such a device must incorporate a mechanism for tuning the NV resonance frequency (by Stark-shift tuning, for example [25]). Cavity tuning by some means other than temperature will also most likely be needed.

3. Spontaneous emission modification in hybrid cavities

Consider a single NV center at position $\mathbf{r}_{NV}$ embedded within a diamond crystal with effective refractive index n_d, adjacent to an optically resonant dielectric structure (such as a microdisk or photonic crystal cavity) with refractive index n_c. We assume that the dipole moment of the NV center is aligned with the polarization vector of the evanescent field emerging from the cavity, the cavity quality factor satisfies $Q \gg 1$ for the mode of interest, and we neglect dispersion in both materials. For the zero-phonon transition of the NV center with angular frequency ω_{ZPL} (assumed to be resonant with the cavity mode), single-photon coupling strength g_{ZPL}, and spontaneous emission rate $\gamma_{ZPL} = 2\pi \times 0.35$ MHz (derived from [32]), the ratio g_{ZPL}^2/γ_{ZPL} is given by Weisskopf–Wigner spontaneous emission theory as [17, 33]

$$\frac{g_{ZPL}^2}{\gamma_{ZPL}} = \frac{3}{16\pi^2}\frac{\lambda^3}{n_d^3}\frac{n_d^2\,|\mathbf{E}(\mathbf{r}_{NV})|^2}{\int d^3\mathbf{r}\,\epsilon(\mathbf{r})|\mathbf{E}(\mathbf{r})|^2}\,\omega_{ZPL}, \tag{1}$$

where $\mathbf{E}(\mathbf{r})$ is the electric field of the cavity mode of interest, $\mathbf{E}(\mathbf{r}_{NV})$ is the electric field at the NV site, and $\epsilon(\mathbf{r})$ is the dielectric constant. The factor of n_d^2 in the numerator enters through the per-photon electric field strength in bulk diamond, while the factor of n_d^3 in the denominator arises from the photon density of states. The integral in the denominator enters through the per-photon electric field strength of the cavity mode. Using a standard definition of mode volume,

$$V = \frac{\int d^3\mathbf{r}\,\epsilon(\mathbf{r})|\mathbf{E}(\mathbf{r})|^2}{\epsilon(\mathbf{r}_{max})|\mathbf{E}(\mathbf{r}_{max})|^2}, \tag{2}$$

where $\mathbf{E}(\mathbf{r}_{max})$ and $\epsilon(\mathbf{r}_{max}) = n_c^2$ are the maximum field strength in the cavity and the dielectric constant at the location of that maximum, respectively, we obtain the spontaneous emission enhancement factor

$$F_{SE} = \frac{4g_{ZPL}^2}{\kappa\gamma_{total}} = \frac{3}{4\pi^2}\frac{\lambda^3}{n_c^3}\frac{Q}{V}\frac{n_c}{n_d}\left|\frac{\mathbf{E}(\mathbf{r}_{NV})}{\mathbf{E}(\mathbf{r}_{max})}\right|^2\frac{\gamma_{ZPL}}{\gamma_{total}}, \tag{3}$$

where κ is the cavity photon decay rate, $Q \equiv \omega_{ZPL}/\kappa$, and $\gamma_{total} = 2\pi \times 13$ MHz [34] is the total spontaneous emission rate including emission into the phonon sidebands.

The expression given in equation (3) for the total on-resonance spontaneous emission enhancement factor in the weak-coupling limit is similar to the Purcell formula $F_{SE} = 3Q\lambda^3/4\pi^2V$ [35] with some additional factors needed to describe bulk systems with evanescent coupling and multiple optical transitions. The factor $\gamma_{ZPL}/\gamma_{total}$ is important for NV centers since only 3% of the total spontaneous emission branches into the zero-phonon line. If we omit this factor, we obtain instead the enhancement factor for the spontaneous emission rate through the zero-phonon line alone.

In later sections, when we examine hybrid bulk diamond/gallium phosphide (GaP) cavity systems, our mode volume computations take both bulk dielectrics into account, so it is sufficient to set $n_c = n_{GaP}$ in equation (3) to determine the modified Purcell factor for cavity-QED applications.

However, in the cavity geometry discussed in section 4, the evanescent field emerges from a silica microdisk into a diamond nanoparticle with dimensions smaller than an optical wavelength. In this case our simulations (which usually incorporate cylindrical symmetry) ignore the nanoparticle, and we compute the external field in vacuum. The nanoparticle can then be approximated as a small dielectric sphere with refractive index n_d embedded in a uniform external electric field, and the Purcell factor is reduced by the usual factor that accounts for the ratio of the internal and external fields:

$$F_{SE} = \frac{4g_{ZPL}^2}{\kappa\gamma_{bulk,total}} = \frac{3}{4\pi^2}\frac{\lambda^3}{n_c^3}\frac{Q}{V}\frac{n_c}{n_d}\left(\frac{3}{2+n_d^2}\right)^2\left|\frac{\mathbf{E}(\mathbf{r}_{NV})}{\mathbf{E}(\mathbf{r}_{max})}\right|^2\frac{\gamma_{ZPL}}{\gamma_{total}}, \quad (4)$$

where in this case $n_c = n_{glass}$. Note that here $\gamma_{bulk,total}$ refers to the total spontaneous emission rate for an NV center in bulk diamond. If we wish to compare the spontaneous emission rate for a nanoparticle coupled to a microdisk with the rate $\gamma_{np,total}$ for a nanoparticle surrounded by vacuum, the enhancement factor (and thus the ZPL collection efficiency) will be larger, since the spontaneous emission rate in nanoparticles is smaller than in bulk diamond [36].

4. Coupling single NV centers in diamond nanoparticles to waveguide-coupled cavities

4.1. Introduction

As discussed above, several approaches have been pursued recently with the aim of coupling NV centers to cavities for quantum information processing applications. Of these approaches, the simplest from a fabrication viewpoint is to couple a nanoparticle containing NV centers to a non-diamond cavity. This route is attractive in that many types of microcavities made from a variety of materials can be used, as long as the nanoparticle can be properly positioned relative to the cavity mode [37, 11, 15]. The main drawback of this approach, as will be discussed below, is the poor spectral properties of NV centers found in nanoparticles.

In this section we describe a low temperature experiment that demonstrated coupling of the zero-phonon line (ZPL) of a single NV center to a silica microdisk, combined with extraction of this light from the microdisk using a tapered optical fiber, all at liquid helium temperatures. In similar experiments, single or few NV center cavity coupling was reported, but previous work has been restricted to room temperature operation [11, 15] or has not demonstrated cavity–waveguide coupling [37].

4.2. Experiment

Silica microcavities 20 μm in diameter were fabricated using conventional optical lithography, wet etching and dry etching techniques. The disks were first defined by a photo-resist mask on a 1.6 μm thermal oxide layer on a silicon wafer. The oxide was next etched in an HF/NH_4F solution. A second lithography step and Bosch etch were used to create 50 μm pedestals beneath the microdisks. Finally, the silicon under the edges of the disks was etched in KOH. An SEM image of a final microdisk is shown in figure 3(a). Initial room temperature quality (Q) factors of the disks were 40 000. However, after the deposition of the nanoparticles and tapered fiber contact at low temperature the final Qs decreased to 2000–3000.

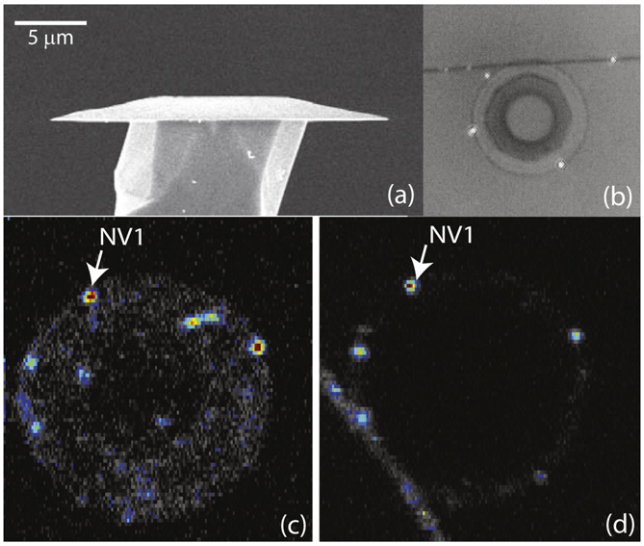

Figure 3. (a) SEM image of a silica microdisk. (b) Optical image of a microdisk coupled to a tapered fiber. Scatter off of three diamond nanoparticles can be observed at the edge of the disk. (c) Scanning confocal image of a silica microdisk showing the location of NV1. Excitation and collection is from the top of the disk. (d) Same as (c) except collection is now through the tapered fiber. The tapered fiber is visible in the lower left corner of the image.

Commercial diamond nanoparticles (Diamond Innovations) with diameters less than 250 nm were suspended in isopropanol and centrifuged to obtain particles with a mean diameter of 70 nm. The silica microdisk sample was then dipped into the diamond suspension and dried on a hotplate at 100 °C. The majority of the particles dried right at the edge of the microdisk. In figure 3(b) scattering from three deposited nanoparticles is clearly observed when 637 nm light is coupled resonantly from a tapered fiber to a microdisk at room temperature.

Confocal photoluminescence (PL) spectroscopy was performed at 17 K in order to identify nanoparticles with NV centers. A 1 μm focused laser spot at a wavelength of 532 nm was scanned over the top of the disk while photoluminescence (PL) from the broadband phonon sidebands (650−800 nm) was also collected from the top. In figure 3(c) several NV centers can be observed at or near the edge of the disk. NV–cavity coupling was then demonstrated by collecting PL through a tapered fiber that was coupled to the microdisk. Figure 3(d) shows an optical image that was obtained by exciting with 532 nm light from the top of the disk and collecting the phonon sideband emission through the tapered fiber. The relative brightness of each nanoparticle in this image differs from that in figure 3(c) because each nanoparticle couples differently to the microdisk.

Once a nanoparticle containing an NV center is identified, such as NV2 in figure 4(a), a photon-counting autocorrelation measurement can be performed to confirm that only a single

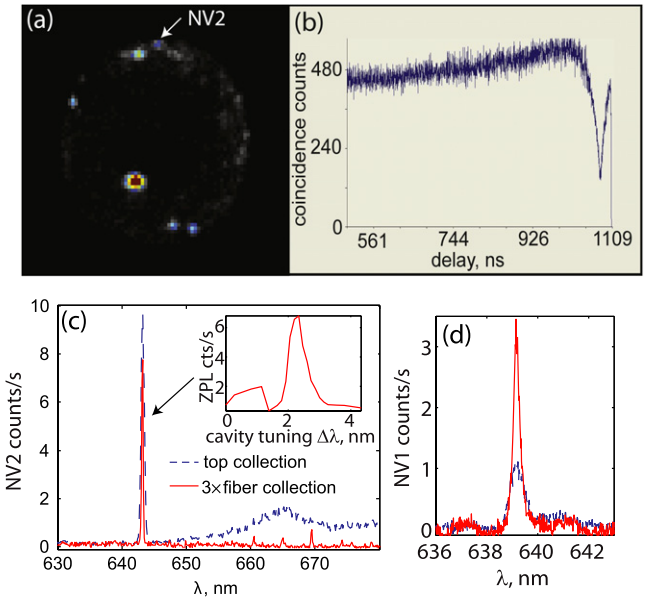

Figure 4. (a) Confocal image of a silica microdisk showing NV2. (b) Measured autocorrelation function for photons emitted from NV2. (c) Low resolution PL spectra of NV2. The cavity (NV) FWHM linewidth for this system was 0.23 nm (0.54 nm). *Inset:* ZPL intensity of NV2 as a function of cavity tuning. (d) High resolution PL spectra of NV1. The cavity (NV) linewidth for this system was 0.27 nm (0.62 nm).

NV is present. The minimum in the autocorrelation curve for NV2 in figure 4(b) is less than half of the maximum value, indicating that the emitted light originates predominantly from a single NV center.

In order to couple the narrow ZPL line to the microcavity it is necessary to tune the cavity. Cavity tuning was achieved by condensing small amounts of nitrogen gas onto the cavity surface, similar to the procedure described in [38]. The frozen gas provides a small change in the cavity mode's effective refractive index, thus shifting the resonance to longer wavelength. Figure 4(c) shows PL spectra of NV2, excited with 532 nm light, and collected through the tapered fiber when the cavity is on resonance with the NV center. The bright ZPL peak at 642 nm can be observed as well as weaker peaks in the phonon sideband region ($\lambda > 650$ nm). For comparison a PL spectrum of NV2 collected from the top of the microdisk is also plotted. The cavity can be tuned over several nanometers using the condensed gas technique. In figure 4(c) *inset* the ZPL intensity as a function of the cavity tuning is plotted for approximately one free spectral range. The coupling of the ZPL line to two cavity modes can be clearly observed.

For NV2 the ZPL collection efficiency per unit frequency is approximately three times less than the collection efficiency through the top objective (NA = 0.55, total system collection efficiency was ∼3%). This is most likely due to poor coupling between the NV center and the cavity mode. However, for NV1, the per-unit-frequency collection efficiency of the ZPL through the tapered fiber is approximately three times higher than for top collection, as shown figure 4(d).

4.3. Outlook for nanoparticle–cavity systems

While the above results clearly demonstrate coupling between the zero-phonon line of a single NV center and a waveguide-coupled cavity at cryogenic temperature, no significant enhancement of the total spontaneous emission rate could be expected given the experimental parameters. In the nanoparticle/silica microdisk system, the total spontaneous emission rate enhancement factor relative to bulk diamond is given by equation (4). The overall performance of these particular devices was limited by the large mode volume V and small Q of the cavities, and also by the poor spectral properties of the NV centers found in the nanoparticles. For our cavities, we estimate the mode volume to be $\sim 90(\lambda/n_{\mathrm{glass}})^3)$ with $|\mathbf{E}(\mathbf{r}_{\mathrm{NV}})/\mathbf{E}(\mathbf{r}_{\mathrm{max}})| = 0.7$ based on numerical simulations. If Qs of approximately 10^6 could be achieved, F_{SE} on the order of 1 could in principle be obtained with this system, if the ZPL width were narrow enough to fit within the cavity resonance linewidth. $F_{\mathrm{SE}} = 1$ corresponds to a 30-fold increase of emission into the ZPL. To achieve even larger enhancements a significant decrease in the mode volume is necessary. This is not possible with the current geometry, although smaller mode volumes are possible in photonic crystal or micropillar cavities [39, 40].

Experimentally, it should be possible to improve Q by orders of magnitude by improving the fabrication processes, by obtaining a better vacuum inside of the cryostat, and through more precise positioning of the tapered fiber. Integration of nanoparticles containing NV centers with cavities having much higher Q has been demonstrated in other recent experiments [37, 15], and it has also been shown that a high Q can be maintained at low temperature in a vacuum cryostat, at least for longer wavelengths [38]. Of more fundamental concern are the spectral properties of NV centers in diamond nanoparticles. Equation (4) assumes that the ZPL is narrow compared with the cavity linewidth. Once the linewidth of the radiation source greatly exceeds that of the cavity, further increases in Q no longer increase the spontaneous emission rate. In figure 4(d), we see that the experimental NV linewidth corresponds to a Q of only ∼1000. Thus, while the cavity Qs were low in this experiment, increasing them would have little benefit unless the NV characteristics could also be improved.

The nanoparticles used in the above experiment were chosen for their relatively high intrinsic NV concentration, which provided a high probability of finding an NV center in any randomly chosen sub-100 nm particle. This high probability allowed nanoparticles to be positioned onto the microdisk edges in a relatively simple way, avoiding the need for a more laborious 'pick 'n place' technique [15, 39, 41] in which special particles are selectively placed onto the microdisk edge. However, it is clear that to make further progress we must search for nanoparticles with improved properties. A narrow ZPL (16 MHz) was recently reported in a nanoparticle which was obtained by mechanically crushing diamond [42]. Although the yield using this technique was low, and additionally the exact size of the 'good' nanoparticle studied was undetermined, at least in principle narrow lines from nanoparticle diamond appear obtainable.

An additional problem for any quantum network application requiring indistinguishable photons from separate NV centers is the large inhomogeneous broadening (several THz) typically seen in nanoparticles, as shown in figure 5(a). This inhomogeneous broadening is most likely due to the different strain fields found in nanoparticles of different shapes and sizes. Figures 5(b)–(d) demonstrate the broadening that occurs when diamond is mechanically crushed to create nanoparticles. Figure 5(b) is a spectrum obtained from CVD diamond (Element 6) which has been irradiated with 2 MeV electrons at a dose of 3×10^{16} cm^{-2} and annealed at 875 °C for 2 h to form NV centers. From PL measurements, the estimated NV density in the sample before crushing was 2×10^{15} cm^{-3}. As seen from the spectra the inhomogeneous broadening in the bulk crystal is quite narrow, and from PLE spectroscopy the inhomogeneous ZPL width was estimated to be ∼10 GHz. This sample was then mechanically crushed. A typical spectrum from a micron-sized particle is shown in figure 5(c). Although many of the individual lines from single NV centers appear sharp, the inhomogeneous broadening is now ∼8 nm, or 6000 GHz. The crushed powder was then centrifuged to select for smaller nanoparticles, and PL spectra were obtained from particles smaller than 500 nm. Approximately 10% of the particles exhibited spectra with linewidths at or close to the spectrometer resolution limit. SEM images showed that the smallest particles containing sharp ZPL lines were all greater than 200 nm in size (see figure 5(d)) even though approximately 1 NV per 100 nm particle was expected. PLE scans of the narrow NV transitions exhibited large spectral diffusion (5 GHz or greater) in all cases. The results of this study suggest that mechanical crushing is not a viable way to obtain homogeneous and spectrally stable NV centers in nanoparticles, and alternative methods will have to be explored. Possible alternatives include nanomilling techniques applied to bulk diamond [43] or growing CVD nanocrystals directly onto a cavity [44]. If good spectral properties can be obtained by one of these methods, then the nanoparticle–cavity system may again be considered as a promising approach for NV-based QIP applications.

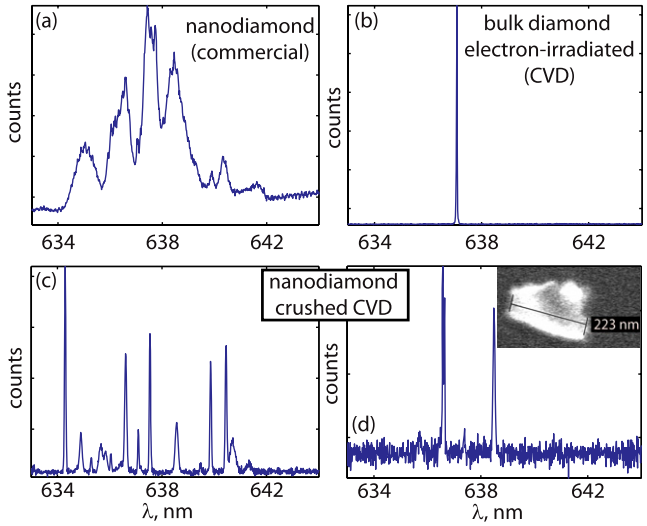

Figure 5. (a) NV PL spectra from a single Diamond Innovations 250 nm nanoparticle. (b) NV PL from electron-irradiated CVD single-crystal diamond. (c) NV PL from a diamond microparticle obtained by mechanically crushing the sample shown in (b). (d) Same as (c) but from a 200 nm nanoparticle. *Inset*: SEM image of the 200 nm nanoparticle.

5. Hybrid nanophotonics for evanescent coupling to single-crystal diamond

5.1. Introduction

Nitrogen-vacancy centers exhibiting the longest measured electron spin coherence lifetimes and the narrowest measured inhomogeneous and homogeneous optical linewidths are found in high-purity, single-crystal diamond samples. Although lithography and reactive ion etching allow single-crystal diamond surfaces to be patterned with high-aspect-ratio features in two dimensions [10, 14, 18], controlling the vertical refractive index profile remains challenging. This control is necessary for optical waveguiding and confinement, and in other material systems is typically achieved either by fabricating nanophotonic devices from multiple layers, so that a thin waveguiding layer is supported by a lower refractive index substrate, or else by growing the waveguiding layer on top of a sacrificial layer which can be selectively removed during the fabrication process.

In hybrid nanophotonic devices, a waveguiding layer is combined with an 'active' cladding or substrate whose optical properties are of interest. The optical modes of the device are primarily confined within the waveguiding layer, but interact evanescently with the adjacent active layer. Hybrid device geometries have recently been used to realize silicon-III/V microlasers [45]. In the approach described below, we have combined a high refractive index waveguide layer with a single-crystal diamond substrate containing NV centers near the diamond surface. The waveguiding layer is fabricated from a GaP film, which at 637 nm has a refractive index $n_{\mathrm{GaP}} \sim 3.3$ and is optically transparent. Since $n_{\mathrm{GaP}} > n_{\mathrm{d}} \sim 2.4$, GaP films on a diamond substrate can support bound modes, and low-loss optical waveguides can be created by patterning the GaP along one dimension. As shown below, by patterning the GaP film in two dimensions, small V, high Q optical microcavities can be realized in this system and can be coupled evanescently to NV centers near the diamond surface.

5.2. Creating NV centers near a single-crystal diamond surface

Synthetic NV centers are often created using either ion implantation or irradiation followed by annealing [46–51]. Ion implantation is used to create carbon vacancies or introduce nitrogen impurities directly into the diamond lattice [52–55], and the choices of particle and acceleration voltage determine the initial vertical distribution of vacancies. Annealing is performed at temperatures (typically 600–1000 °C) where vacancies become mobile and can combine with nitrogen impurities to form NV centers. Vacancies can also recombine with self-interstitials [47, 56, 57] (implantation produces one

interstitial carbon for each vacancy), can join together to form extended defects [58], or can become trapped at either dislocations or the crystal surface [59]. The question of how far vacancies diffuse vertically from the initially damaged layer at temperatures optimized to create NV centers is of critical importance for designing optical structures that use evanescent coupling.

We have performed etching experiments followed by photoluminescence (PL) measurements that reveal the vertical distribution of optically active NV centers produced using ion implantation and annealing to convert native nitrogen into NV centers [60]. We used two samples of (100)-oriented bulk diamond: an HPHT crystal with a high average native nitrogen concentration (30–100 ppm), and a CVD crystal with a nitrogen concentration below 1 ppm. After implantation with different doses of 200 keV Ga ions, both samples were annealed at 925 °C in an H_2/Ar forming gas for 3 h. For each sample, we etched a layer of diamond in the z direction to a depth ζ, excited the remaining NV centers produced by ion implantation and annealing with weak laser light at 532 nm, and collected the resulting PL intensity $\sigma(\zeta)$ using bandpass filters to select wavelengths over the range 647–804 nm for detection of the NV^- phonon sidebands. Since the depth of focus of our optical setup is much larger than 1 μm in diamond, this PL measurement integrates contributions from all of the remaining centers, so that the measured intensity should depend on the initial NV concentration $\rho(z)$ (before etching) according to,

$$\sigma(\zeta \geqslant 0) = \int_{\zeta}^{\infty} \mathrm{d}z\, \eta(z-\zeta)\, \rho(z). \qquad (5)$$

Here $\eta(z)$ is a spontaneous emission collection factor that arises from the interaction of the NV dipole with the dielectric boundary at the interface of the diamond surface and air. To obtain the most accurate estimate of $\rho(z)$ we must solve a deconvolution problem, as discussed in [60]. In figure 6, the final vertical density of NV centers $\rho(z)$ obtained by inverting equation (5) is plotted for the two samples, including both high nitrogen and low nitrogen sectors for the HPHT sample. From these results we find that the vertical distance over which vacancies diffuse to form NV centers is only a few hundred nanometers, even for a fairly high annealing temperature of 925 °C. In high nitrogen diamond, the dense layer of NV^- extends all the way to the surface, and thus NV centers may couple evanescently to optical structures placed onto the surface. However, in moderately low nitrogen (∼1 ppm) diamond, if the implantation dose is chosen to maximize the total PL intensity measured from above, then we find little NV^- within 100 nm of the surface, and thus most of the observed photoluminescence corresponds to NV centers that cannot couple evanescently to optical structures.

In [60] we proposed, based on spectroscopic measurements, that the lack of fluorescence near the surface in the low nitrogen material, as seen in figures 6(b), (c), occurs due to electronic depletion effects, such that no electrons are available to form negatively-charged NV^-. The observed behavior can be explained by the presence of electronic acceptors near the surface, which could consist of impurities or defects

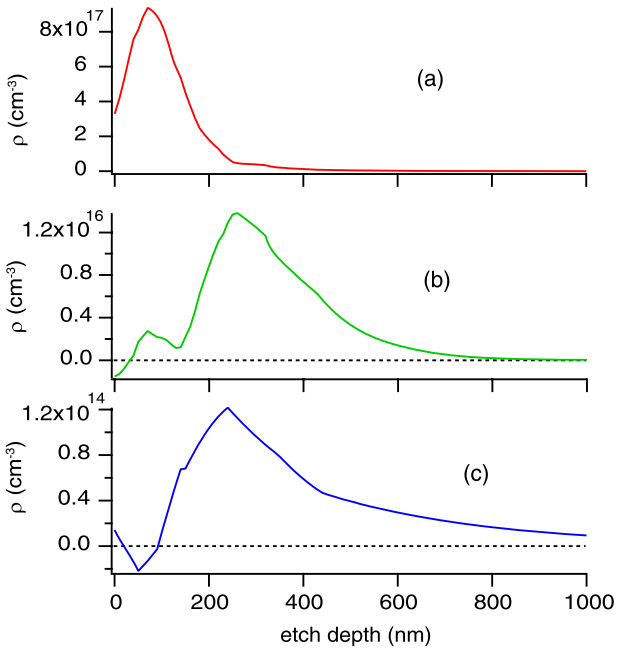

Figure 6. (a)–(c) NV concentration versus depth for three different diamond samples [60].

introduced through the ion implantation and annealing, or damage originally present in the sample. Controlling such effects will be important in finding improved methods to couple dense ensembles of NV centers to optical structures on a diamond surface, and also for the fabrication of single negatively-charged NV centers in ultra-pure diamond, where electronic depletion layers thicker than 1 μm are possible.

The results presented here are most relevant to the approach in which ion implantation is used to create carbon vacancies that combine with existing nitrogen upon annealing. This approach is adequate for creating dense layers of NV centers near a surface which can be used for initial tests of nanophotonic devices. Currently, effort is underway to optimize nitrogen implantation approaches that are more suitable for creating single NV centers near a diamond surface.

5.3. Design and simulation of GaP–diamond nanophotonic devices

Hybrid GaP–diamond nanophotonic devices were first investigated in [17], where a thin GaP film (thickness $t \sim$ 120–250 nm) was patterned with long ridges and attached to a diamond substrate. Waveguiding was observed in the resulting GaP–diamond ridge waveguides, and coupling between NVs near the GaP–diamond interface and waveguide modes was studied as a function of t. A waveguide loss of $< 72 \pm 8$ dB cm^{-1} was observed in these studies, indicating that the system is suitable for microcavities with quality factor $Q >$ 20 000.

In a hybrid microcavity, maximizing the Q/V ratio is hindered by radiation loss into the diamond substrate, which has a moderately high refractive index. Compared with a lower-refractive-index SiO_2 or air substrate, a diamond substrate expands the light cone into which a microcavity can

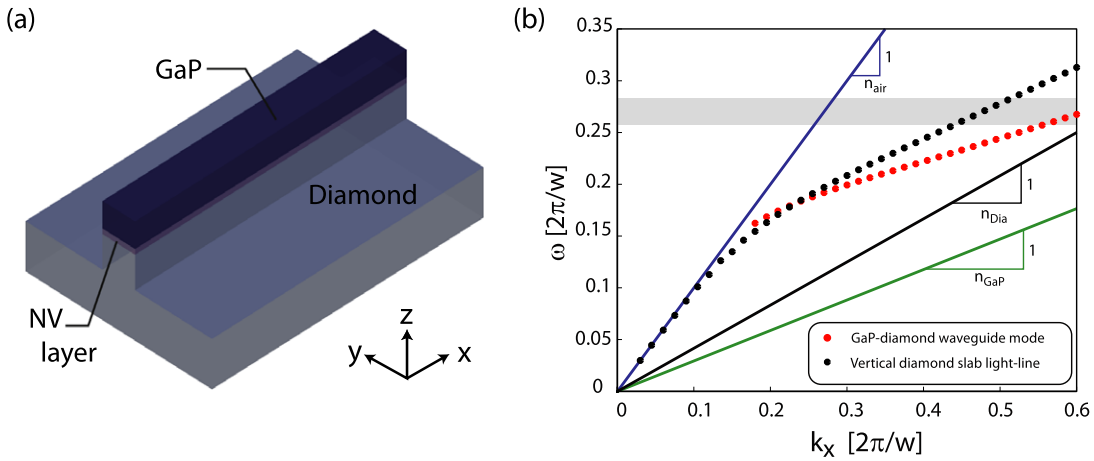

Figure 7. (a) Schematic of a hybrid GaP–diamond nanowire waveguide. (b) Nanowire waveguide dispersion (mode frequency, ω, versus wavenumber, k_x), and relevant material lightlines. The vertical diamond slab lightline is the dispersion of the lowest-order mode of a diamond slab of width w. The wavelength range associated with emission from the phonon sidebands of an NV^- is indicated by the shaded gray region.

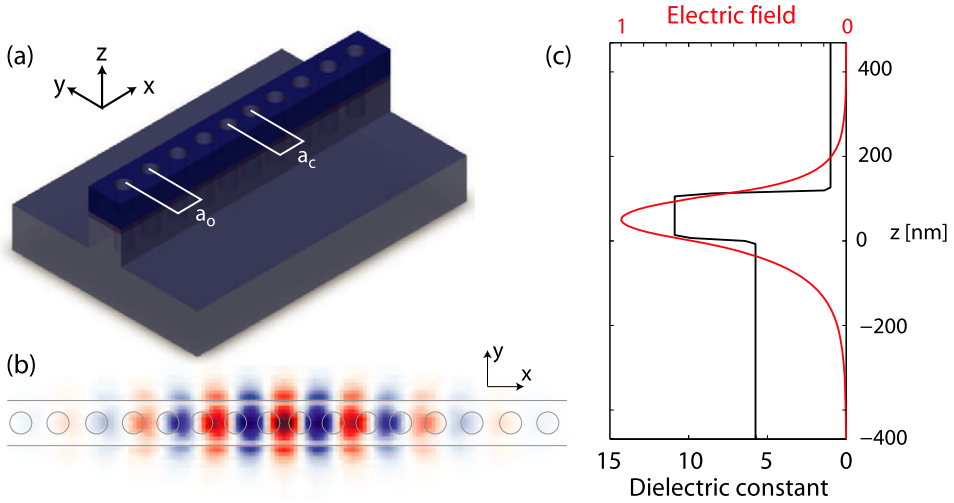

Figure 8. (a) Schematic of a hybrid GaP–diamond photonic crystal nanocavity. The hole spacing, a, is varied gradually from $a_o = 160$ nm to $a_c = 140$ nm, as described in [19]. (b) Simulated field profile and cavity outline (top view). (c) Electric field amplitude and dielectric constant cross-section, taken through the nanocavity center.

radiate. For a given acceptable device quality factor Q_i, this increases the minimum device dimension for which $Q > Q_i$.

Substrate leakage can be reduced by extending the waveguide layer patterning into the diamond, effectively renormalizing the spectrum of substrate radiation modes. Figure 7 illustrates this mechanism for a simple GaP–diamond nanowire waveguide of width $w = 180$ nm and thickness $t = 120$ nm, as illustrated in figure 7(a). The band structure for the lowest-order waveguide mode, calculated using finite difference time domain simulations (FDTD), is shown in figure 7(b). At an operating wavelength of 637 nm, the waveguide mode dispersion lies above the diamond lightline, indicating that the mode can radiate into the substrate. However, if the GaP sidewalls are extended into the diamond substrate, the relevant substrate lightline becomes that of a thin vertical diamond slab of width w. This lightline is also shown in figure 7(b), and at 637 nm lies above the nanowire waveguide dispersion. This indicates that in the limit that the diamond etch depth $h \gg (637\text{ nm})/n_d$, the nanowire mode will not radiate into the substrate.

This nanowire waveguide is the underlying structure of a photonic crystal heterostructure nanocavity proposed in [19]. The waveguide is patterned with air holes whose spacing is slowly varied to form a defect which supports localized optical modes [61–63]. Figure 8(a) shows a schematic of the proposed design, and the FDTD simulated electric field profile of an ultrahigh-Q/V mode supported by this device is shown in figure 8(b). This mode is predominantly TE polarized (electric field along y axis), and has $V < 0.52(\lambda/n_{GaP})^3$, and radiation limited $Q > 1.5 \times 10^6$ for a diamond etch depth $h = 600$ nm. As shown in figure 8(c), although the field maximum is located within the GaP layer, a significant field amplitude extends evanescently into the diamond. Using the equations from section 3, we predict that for an NV center optimally located

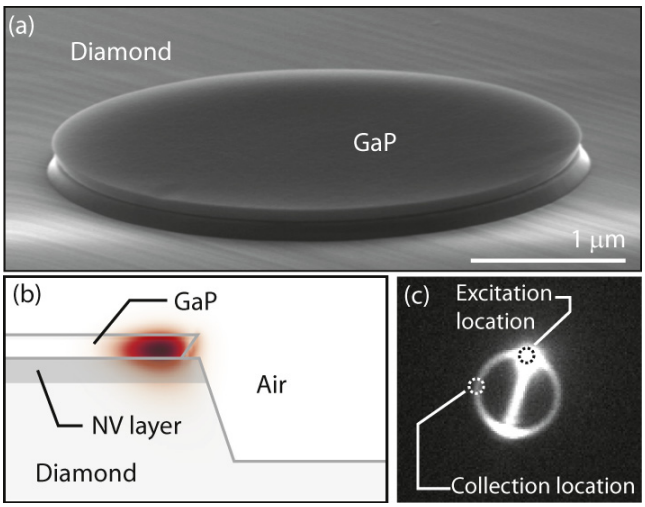

Figure 9. (a) SEM image of a hybrid GaP–diamond microdisk. (b) Simulated field profile of the fundamental TE-like mode of a hybrid GaP–diamond microdisk. (c) Widefield CCD image of the photoluminescence from a hybrid GaP–diamond microdisk.

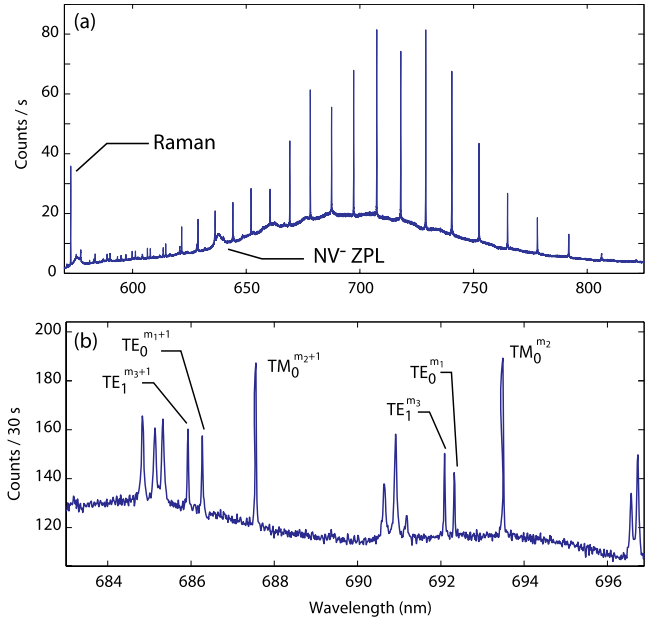

Figure 10. (a) Photoluminescence spectrum from a hybrid microdisk with diameter $d \sim 4.5$ μm, GaP thickness $t \sim 130$ nm, and diamond etch depth $h \sim 600$ nm. (b) High resolution spectrum for a hybrid microdisk with $t \sim 250$ nm, $d \sim 4.5$ μm, and $h \sim 600$ nm. Modes from the three lowest-order families of whispering-gallery-mode resonances are identified. Excitation power ∼2.5 mW.

at the diamond surface, $g_{\mathrm{ZPL}} = 2\pi \times 2.25$ GHz and $F_{\mathrm{SE}} = 4900$. In the realistic scenario where imperfect fabrication and material loss limit Q to 2×10^4, and the NV is positioned 50 nm below the surface, we estimate $F_{\mathrm{SE}} > 16$, indicating that efficient collection of NV spontaneous emission is still possible with an imperfect device.

5.4. Experimental demonstration of GaP–diamond microdisk cavities

This hybrid device geometry can also be applied to whispering-gallery-mode microcavities, such as microdisks and microrings. Microdisks trade off larger V for simpler-to-fabricate geometries. As described in [18], we have fabricated GaP microdisks, which were then attached to single-crystal diamond substrates containing a high density of NVs near the sample surface. Using an oxygen and argon based reactive ion etching process, the GaP sidewalls were then extended into the diamond substrate. Figure 9(a) shows an SEM image of a fabricated hybrid GaP–diamond microdisk, and figure 9(b) shows the vertical cross-section of a whispering-gallery mode supported by this structure, calculated from a finite difference time domain simulation. Optical coupling between NVs near the diamond surface and the GaP microdisk was studied experimentally using a micro-photoluminescence (μ-PL) apparatus. A green (532 nm) excitation source excited NVs near the microdisk edge through a high-NA microscope objective. Figure 9(c) shows a widefield CCD image of the resulting microdisk PL, and clearly illustrates that a fraction of the NV emission was coupled into whispering-gallery modes of the hybrid microdisk. Light radiated from the microdisk edge at an azimuthal position rotated ∼90° from the excitation location, as indicated in figure 9(c), was sent to a spectrometer.

Photoluminescence spectra from typical hybrid GaP–diamond microdisks are shown in figure 10. Figure 10(a) shows a spectrum from a $d \sim 4.5$ μm diameter device with a $t \sim 130$ nm GaP thickness. Broad background emission from NV^- color centers can be identified from the prominent hump near 637 nm. Superimposed upon this background are sharp resonances corresponding to NV emission coupled into microdisk whispering-gallery modes, and then radiated and measured by the spectrometer. The resonances are regularly spaced, and are associated with the fundamental TE-like mode of the microdisk, with varying azimuthal quantum number. Figure 10(b) shows a high resolution spectrum from a device with a larger GaP thickness, $t \sim 250$ nm. This device supports high-Q, higher-order transverse modes, resulting in a more complicated spectrum, analyzed in more detail in [18]. Measurement of the linewidth of these resonances is limited by the spectrometer resolution, corresponding to a lower bound of $Q > 25\,000$. An upper limit of $Q < 75\,000$ for these resonances was measured by placing an adjustable interferometer at the spectrometer input to determine the coherence length of light emitted from the unresolved microdisk resonance. The radiation limited Q calculated with FDTD for this is greater than 10^6, indicating that material absorption or surface scattering limits the measured Q. The minimum mode volume of the devices studied here is $V \sim 18(\lambda/n_{\mathrm{GaP}})^3$. For the best devices, we estimate that for an optimally placed NV center having a zero-phonon line that is narrow compared with the cavity resonance, the spontaneous emission rate into the zero-phonon line could be enhanced by a factor of 17, while the total spontaneous emission rate would increase by an additional 50%. Further reduction of the mode volume, before radiation loss limits Q, will be possible in future devices, hopefully leading to larger Purcell enhancements. These results also indicate that

fabrication and demonstration of the photonic crystal device proposed above with $Q > 10^4$ may be possible.

6. Summary

In conclusion, we have investigated several approaches for coupling nitrogen-vacancy centers to optical microcavities. In the nanocrystal-based approach, we have shown that the zero-phonon line from a single NV center can be coupled to a SiO_2 microdisk cavity mode at low temperature, and this light can be extracted through a tapered optical fiber. In the bulk diamond approach, we have shown that GaP microdisk cavities can be placed onto a diamond surface with quality factors $Q > 25\,000$, and based on numerical simulations we expect also that nanowire photonic crystal cavities with similar quality factors but smaller mode volumes can be realized. In the GaP approach the Q/V ratios are already high enough that in theory a large enhancement of the zero-phonon spontaneous emission rate is possible at low temperature, for an optimally placed NV center. The main remaining practical challenges in both approaches concern the properties of the NV centers themselves. In nanoparticles, random strain fields produce a huge inhomogeneous broadening, and even obtaining single nitrogen-vacancy centers with consistently narrow optical linewidths in nanocrystal sizes below 200 nm remains an unsolved problem. In bulk diamond, obtaining NV centers with narrow optical linewidths within 50 nm of a diamond surface is also challenging, but appears more hopeful, and is the subject of current research.

This material is based upon work supported by the Defense Advanced Research Projects Agency under Award No. HR0011-09-1-0006 and The Regents of the University of California.

References

[1] Twitchen D J, Whitehead A J, Coe S E, Isberg J, Hammersberg J, Wikstrom T and Johansson E 2004 High-voltage single-crystal diamond diodes *IEEE Trans. Electron Devices* **51** 826–8

[2] Zaitsev A M 2001 *Optical Properties of Diamond: A Data Handbook* (Berlin: Springer)

[3] Balasubramanian G *et al* 2009 Ultralong spin coherence time in isotopically engineered diamond *Nat. Mater.* **8** 383–7

[4] Jelezko F, Gaebel T, Popa I, Domhan M, Gruber A and Wrachtrup J 2004 Observation of coherent oscillation of a single nuclear spin and realization of a two-qubit conditional quantum gate *Phys. Rev. Lett.* **93** 130501

[5] Childress L, Gurudev Dutt M V, Taylor J M, Zibrov A S, Jelezko F, Wrachtrup J, Hemmer P R and Lukin M D 2006 Coherent dynamics of coupled electron and nuclear spin qubits in diamond *Science* **314** 281–5

[6] Childress L, Taylor J M, Sorensen A S and Lukin M D 2005 Fault-tolerant quantum repeaters with minimal physical resources and implementations based on single-photon emitters *Phys. Rev.* A **72** 52330

[7] Benjamin S C, Browne D E, Fitzsimons J and Morton J J L 2006 Brokered graph-state quantum computation *New J. Phys.* **8** 141

[8] Wang C F, Hanson R, Awschalom D D, Hu E L, Feygelson T, Yang J and Butler J E 2007 Fabrication and characterization of two-dimenstional photonic crystal microcavities in nanocrystalline diamond *Appl. Phys. Lett.* **91** 201112

[9] Park Y-S, Cook A K and Wang H 2006 Cavity QED with diamond nanocrystals and silica microspheres *Nano Lett.* **6** 2075–9

[10] Hiscocks M P, Ganesan K, Gibson B C, Huntington S T, Ladouceur F and Prawer S 2008 Diamond waveguides fabricated by reactive ion etching *Opt. Express* **16** 19512–9

[11] Schietinger S, Schroder T and Benson O 2008 One-by-one coupling of single defect centers in nanodiamonds to high-q modes of an optical microresonator *Nano Lett.* **8** 3911–5

[12] Schietinger S and Benson O 2009 Coupling single NV-centres to high-Q whispering gallery modes of a preselected frequency-matched microresonator *J. Phys. B: At. Mol. Phys.* **42** 114001

[13] Schietinger S, Barth M, Aichele T and Benson O 2009 Plasmon-enhanced single photon emission from a nanoassembled metal–diamond hybrid structure at room temperature *Nano Lett.* **9** 1694–8

[14] Larsson M, Dinyari K N and Wang H 2009 Composite optical microcavity of diamond nanopillar and silica microsphere *Nano Lett.* **9** 1447–50

[15] Barclay P E, Santori C, Fu K-M, Beausoleil R G and Painter O 2009 Coherent interference effects in a nano-assembled diamond nv center cavity-qed system *Opt. Express* **17** 8081–97

[16] Fu K M C, Santori C, Spillane S and Beausoleil R G 2008 Quantum information processing with diamond nitrogen-vacancy centers coupled to microcavities *Proc. SPIE* **6903** 69030M

[17] Fu K-M C, Santori C, Barclay P E, Aharonovich I, Prawer S, Meyer N, Holm A M and Beausoleil R G 2008 Coupling of nitrogen-vacancy centers in diamond to a gap waveguide *Appl. Phys. Lett.* **93** 234107

[18] Barclay P E, Fu K-M C, Santori C and Beausoleil R G 2009 Chip-based microcavities coupled to nitrogen-vacancy centers in single crystal diamond *Appl. Phys. Lett.* **95** 191115

[19] Barclay P E, Fu K-M, Santori C and Beausoleil R G 2009 Hybrid photonic crystal cavity and waveguide for coupling to diamond nv-centers *Opt. Express* **17** 9588–601

[20] Manson N B, Harrison J P and Sellars M J 2006 Nitrogen-vacancy center in diamond: model of the electronic structure and associated dynamics *Phys. Rev.* B **74** 104303

[21] Tamarat P *et al* 2008 Spin-flip and spin-conserving optical transitions of the nitrogen-vacancy centre in diamond *New J. Phys.* **10** 045004

[22] Batalov A, Jacques V, Kaiser F, Siyushev P, Neumann P, Rogers L J, McMurtrie R L, Manson N B, Jelezko F and Wrachtrup J 2009 Low temperature studies of the excited-state structure of negatively charged nitrogen-vacancy color centers in diamond *Phys. Rev. Lett.* **102** 195506

[23] Santori C *et al* 2006 Coherent population trapping in diamond nv centers at zero magnetic field *Opt. Express* **14** 7986–93

[24] Santori C *et al* 2006 Coherent population trapping of single spins in diamond under optical excitation *Phys. Rev. Lett.* **97** 247401

[25] Tamarat Ph *et al* 2006 Stark shift control of single optical centers in diamond *Phys. Rev. Lett.* **97** 083002

[26] Fu K-M C, Santori C, Barclay P E, Rogers L J, Manson N B and Beausoleil R G 2009 Observation of the dynamic Jahn–Teller effect in the excited states of nitrogen-vacancy centers in diamond *Phys. Rev. Lett.* **103** 256404

[27] Fuchs G D, Dobrovitski V V, Hanson R, Batra A, Weis C D, Schenkel T and Awschalom D D 2008 Excited-state spectroscopy using single spin manipulation in diamond *Phys. Rev. Lett.* **101** 117601

[28] Neumann P *et al* 2009 Excited-state spectroscopy of single nv defects in diamond using optically detected magnetic resonance *New J. Phys.* **11** 013017

[29] Rogers L J, McMurtrie R L, Sellars M J and Manson N B 2009 Time-averaging within the excited state of the nitrogen-vacancy centre in diamond *New J. Phys.* **11** 063007

[30] Delaney P, Greer J C and Larsson J A 2010 Spin-polarization mechanisms of the nitrogen-vacancy center in diamond *Nano Lett.* **10** 610–4
[31] Cabrillo C, Cirac J I, García-Fernández P and Zoller P 1999 Creation of entangled states of distant atoms by interference *Phys. Rev.* A **59** 1025–33
[32] Davies G 1974 Vibronic spectra in diamond *J. Phys. C: Solid State Phys.* **7** 3797–809
[33] Scully M O and Zubairy M S 1997 *Quantum Optics* (Cambridge: Cambridge University Press)
[34] Collins A T, Thomaz M F and Jorge M I B 1983 Luminescence decay time of the 1.945 eV centre in type Ib diamond *J. Phys. C: Solid State Phys.* **16** 2177–81
[35] Purcell E M 1946 Spontaneous emission probabilities at radio frequencies *Phys. Rev.* **69** 681
[36] Beveratos A, Brouri R, Gacoin T, Poizat J-P and Grangier P 2001 Nonclassical radiation from diamond nanocrystals *Phys. Rev.* A **64** 061802
[37] Wang C F, Choi Y-S, Lee J C, Hu E L, Yang J and Butler J E 2007 Observation of whispering gallery modes in nanocrystalline diamond microdisks *Appl. Phys. Lett.* **90** 081110
[38] Srinivasan K and Painter O 2007 Optical fiber taper coupling and high-resolution wavelength tuning of microdisk resonators at cryogenic temperatures *Appl. Phys. Lett.* **90** 031114
[39] Barth M, Nüsse N, Löchel B and Benson O 2009 Controlled coupling of a single-diamond nanocrystal to a photonic crystal cavity *Opt. Lett.* **34** 1108–10
[40] Zhang Y and Loncar M 2009 Submicrometer diameter micropillar cavities with high quality factor and ultrasmall mode volume *Opt. Lett.* **34** 902
[41] Ampem-Lassen E, Simpson1 D A, Gibson B C, Trpkovski S, Hossain F M, Huntington S T, Ganesan K, Hollenberg L C L and Prawer S 2009 Nano-manipulation of diamond-based single photon sources *Opt. Express* **17** 11287
[42] Shen Y, Sweeney T M and Wang H 2008 Zero-phonon linewidth of single nitrogen vacancy centers in diamond nanocrystals *Phys. Rev.* B **77** 033201
[43] Boudou J-P, Curmi P A, Jelezko F, Wrachtrup J, Aubert P, Sennour M, Balasubramanian G, Reuter R, Thorel A and Gaffet E 2009 High yield fabrication of fluorescent nanodiamonds *Nanotechnology* **20** 235602
[44] Aharonovich I, Zhou C, Stacey A, Treussart F, Roch J-F and Prawer1 S 2008 Formation of color centers in nanodiamonds by plasma assisted diffusion of impurities from the growth substrate *Appl. Phys. Lett.* **93** 243112
[45] Liang D, Fiorentino M, Okumura T, Chang H H, Spencer D T, Kuo Y H, Fang A W, Dai D, Beausoleil R G and Bowers J E 2009 Electrically-pumped compact hybrid silicon microring lasers for optical interconnects *Opt. Express* **17** 20355–64
[46] Davies G and Hamer M F 1976 Optical studies of the 1.945 eV vibronic band in diamond *Proc. R. Soc. Lond.* A **348** 285–98
[47] Davies G, Lawson S C, Collins A T, Mainwood A and Sharp S J 1992 Vacancy-related centers in diamond *Phys. Rev.* B **46** 13157–70
[48] Mita Y 1996 Change of absorption spectra in type-ib diamond with heavy neutron irradiation *Phys. Rev.* B **53** 11360–4
[49] Martin J, Wannemacher R, Teichert J, Bischoff L and Köhler B 1999 Generation and detection of fluorescent color centers in diamond with submicron resolution *Appl. Phys. Lett.* **75** 3096
[50] Waldermann F C *et al* 2007 Creating diamond color centers for quantum optical applications *Diamond Relat. Mater.* **16** 1887–95
[51] Wee T L, Tzeng Y K, Han C C, Chang H C, Fann W, Hsu J H, Chen K M and Yu Y C 2007 Two-photon excited fluorescence of nitrogen-vacancy centers in proton-irradiated type ib diamond *J. Phys. Chem.* A **111** 9379–86
[52] Burchard B, Meijer J, Popa I, Gaebel T, Domhan M, Wittmann C, Jelezko F and Wrachtrup J 2005 Generation of single color centers by focused nitrogen implantation *Appl. Phys. Lett.* **87** 261909
[53] Greentree A D *et al* 2006 Critical components for diamond-based quantum coherent devices *J. Phys.: Condens. Matter* **18** 825
[54] Rabeau J R, Reichart P, Tamanyan G, Jamieson D N, Prawer S, Jelezko F, Gaebel T, Popa I, Domhan M and Wrachtrup J 2006 Implantation of labelled single nitrogen vacancy centers in diamond using n *Appl. Phys. Lett.* **88** 023113
[55] Weis C D *et al* 2008 Single-atom doping for quantum device development in diamond and silicon *J. Vac. Sci. Technol.* B **26** 2596–600
[56] Allers L, Collins A T and Hiscock J 1998 The annealing of interstitial-related optical centres in type ii natural and cvd diamond *Diamond Relat. Mater.* **7** 228–32
[57] Newton M E, Campbell B A, Twitchen D J, Baker J M and Anthony T R 2002 Recombination-enhanced diffusion of self-interstitial atoms and vacancy–interstitial recombination in diamond *Diamond Relat. Mater.* **11** 618–22
[58] Hounsome L S, Jones R, Martineau P M, Fisher D, Shaw M J, Briddon P R and Öberg S 2006 Origin of brown coloration in diamond *Phys. Rev.* B **73** 125203
[59] Nelson R S, Hudson J A, Mazey D J and Piller R C 1983 Diamond synthesis: Internal growth during c^+ ion implantation *Proc. R. Soc. Lond.* A **386** 211–22
[60] Santori C, Barclay P E, Fu K-M C and Beausoleil R G 2009 Vertical distribution of nitrogen-vacancy centers in diamond formed by ion implantation and annealing *Phys. Rev.* B **79** 125313
[61] Notomi M, Kuramochi E and Taniyama H 2008 Ultrahigh-q nanocavity with 1d photonic gap *Opt. Express* **16** 11095
[62] Chan J, Eichenfield M, Camacho R and Painter O 2009 Optical and mechanical design of a 'zipper' photonic crystal optomechanical cavity *Opt. Express* **17** 3802–17
[63] McCutcheon M W and Lončar M 2008 Design of an ultrahigh quality factor silicon nitride photonic crystal nanocavity for coupling to diamond nanocrystals *Opt. Express* **16** 19136